Applications of Photoluminescence Imaging to Dopant and Carrier Concentration Measurements of Silicon Wafers

S. Y. Lim, M. Forster, X. Zhang, J. Holtkamp, M. C. Schubert, A. Cuevas, and D. Macdonald

***Abstract*—Photoluminescence-based imaging is most commonly used to measure the excess minority carrier density and its corresponding lifetime. By using appropriate surface treatments, this high-resolution imaging technique can also be used for majority carrier concentration determination. The mechanism involves effectively pinning the minority excess carrier density, resulting in a dependence of the photoluminescence intensity on only the majority carrier density. Three suitable surface preparation methods are introduced in this paper: aluminum sputtering, deionized water etching, and mechanical abrasion. Spatially resolved dopant density images determined using this technique are consistent with the images obtained by a well-established technique based on free carrier infrared emission. Three applications of the technique are also presented in this paper, which include imaging of oxygen-related thermal donors, radial dopant density analysis, and the study of donor-related recombination active defects. These applications demonstrate the usefulness of the technique in characterizing silicon materials for photovoltaics.**

***Index Terms*—Carrier density, photoluminescence (PL), silicon, surface recombination.**

I. Introduction

KNOWING the concentration of both majority and minority carriers is essential for semiconductor device physics. Recombination processes and device voltage are intimately linked to the *pn* product, and so are many characterization techniques. For example, the physical mechanism underlying luminescence from band-to-band carrier transitions is directly determined by the *pn* product [1]. As such, measurement of the luminescence intensity can provide information about either the majority or the minority carrier concentration. This has been exploited through the use of photoluminescence (PL) imaging for rapid, highly resolved carrier lifetime images [1]. When a wafer is dominated by either a high surface recombination rate [2] or Auger recombination rate [3], PL imaging actually allows measurement of the majority carrier concentration, revealing interesting information about dopant incorporation in silicon ingots. A critical precondition for the former measurements is a uniformly large surface recombination velocity. Although a sufficiently high recombination rate can sometimes be found in as-cut samples, in many cases, additional surface treatment is required. This paper demonstrates a number of suitable sample treatments, ranging from metal coating, chemical etching, and mechanical abrasion, that can achieve the required high surface recombination, as well as ensuring surface homogeneity for accurate majority carrier imaging.

Manuscript received June 26, 2012; revised October 22, 2012; accepted October 30, 2012. Date of publication December 13, 2012; date of current version March 18, 2013. This work was supported by the Australian Research Council.

S. Y. Lim, X. Zhang, A. Cuevas, and D. Macdonald are with the Research School of Engineering, The Australian National University (ANU), Canberra, ACT 0200, Australia (e-mail: siew.lim@anu.edu.au; xinyu.zhang@anu.edu.au; andres.cuevas@anu.edu.au; daniel.macdonald@anu.edu.au).

M. Forster is with the Apollon Solar, Lyon 69002, France (e-mail: forster@apollonsolar.com).

J. Holtkamp and M. C. Schubert are with the Fraunhofer Institut fur Solare Energiesysteme (ISE), 79110 Freiburg, Germany (e-mail: jan.holtkamp@ise.fraunhofer.de; martin.schubert@ise.fraunhofer.de).

Color versions of one or more of the figures in this paper are available online at http://ieeexplore.ieee.org.

Digital Object Identifier 10.1109/JPHOTOV.2012.2228301

II. Theory

A. Photoluminescence Technique

In semiconductors, the measured PL intensity, or count rate, $I_{\rm PL}(\rm s^{-1})$ is proportional to the rate of radiative recombination $R_{\rm rad}$ and is thus proportional to the product of the minority and majority carrier densities:

$$I_{\rm PL} = A_i \cdot B \cdot n \cdot p \tag{1}$$

where A_i is a scaling factor, and B is the radiative recombination coefficient [4]. For p-type silicon, at low injection, when $\Delta n \ll N_A, I_{\rm PL} = A_i \cdot B \cdot \Delta n \cdot N_A$. Similarly, for n-type silicon, when $\Delta p \ll N_D, I_{\rm PL} = A_i \cdot B \cdot \Delta p \cdot N_D$.

Under steady-state conditions, the average excess carrier density $\Delta n_{\rm av}$ is given as $\Delta n_{\rm av} = \tau_{\rm eff} \cdot G$, where $\tau_{\rm eff}$ is the effective minority carrier lifetime, incorporating both bulk and surface recombination, and G is the generation rate.

B. Effective Minority Carrier Lifetime

If the surfaces have such high recombination velocities that recombination there is effectively instantaneous, and if the bulk minority carrier lifetime is sufficiently high (i.e., bulk lifetime larger than the transit time by at least two orders of magnitude will allow dopant density variations of less than 5% to be resolved) [2], then the effective minority carrier lifetime becomes equal to the transit time, defined as the average time required for generated carriers to diffuse to a surface, which for uniformly absorbed steady-state photogeneration is given by [5], [6]

$$\tau_{\rm transit} = \frac{W^2}{12 D_n} \tag{2}$$

where W is the sample thickness, and D_n is the minority carrier (electron) diffusivity. The measured PL in low injection is, therefore, obtained as follows:

$$I_{\mathrm{PL}} = A_i \cdot B \cdot N_A \cdot G \cdot \frac{W^2}{12D_n} \infty N_A \cdot \frac{W^2}{12D_n}. \qquad (3)$$

Since the electron diffusivity D_n is only weakly dependent on doping concentration, a near linear relationship between I_{PL} and N_A can be expected. The slightly superlinear relationship between I_{PL} and N_A arises due to the gradual reduction of the diffusion coefficient with respect to the dopant density, as well as the weak dependence of the radiative recombination coefficient on the dopant density in the range of dopant densities $>10^{15}$ cm^{-3} [7], [8].

C. Numerical Model Predictions

The above analysis is only valid for uniform photogeneration. In the case of monochromatic incident light which is not uniformly absorbed, the carrier concentration will be asymmetrical across the wafer thickness. The imaging system in this study uses 808-nm illumination which corresponds to an absorption depth of 13 μm. Simulations of detected PL intensity which take into account such nonuniform photogeneration profile can be obtained, for example, with QSSModel simulation software [9]. This allows PL modeling for monochromatic incident light of a range of specific wavelengths. By using QSSModel and applying Klaassen's mobility model to obtain the electron diffusivity, the simulation result reveals a near linear relationship between the PL intensity and dopant density due to the effective pinning of τ_{eff} under surface-limited recombination conditions. The detected PL intensity is calculated by assuming a detector quantum efficiency of 40% at 1000 nm, which is then used to determine the quantum efficiency at other wavelengths based on known values for the absorption coefficient, and assuming a planar Si detector, as described in [10]. The modeled results of the above simulation for p-type wafers of three different wafer thicknesses are shown in Fig. 1. A slightly superlinear relationship of $I_{\mathrm{PL}} = A \cdot N_A^{1.1}$ is represented by the fits (solid lines), where A is a thickness-dependent proportionality constant. The slight superlinear nature arises primarily from the dependence of the carrier diffusivity on the doping. This dominant dependence of PL intensity on dopant density allows the dopant density to be measured in a spatially resolved way via the PL method and, therefore, forms the basis for the surface-limited dopant imaging technique.

A limitation of this method is found for materials with regions of low lifetime or highly doped materials of resistivities $<\sim 0.05\ \Omega$.cm [2], where Auger recombination starts to dominate bulk lifetime. In these cases, decoupling of the dopant density and bulk lifetime will involve more complex procedures, which is beyond the scope of this paper.

III. Experimental Details

In this study, PL measurements were obtained with a BT Imaging LIS-R1 system. During measurement, steady-state carrier generation was achieved with an 808-nm laser diode array.

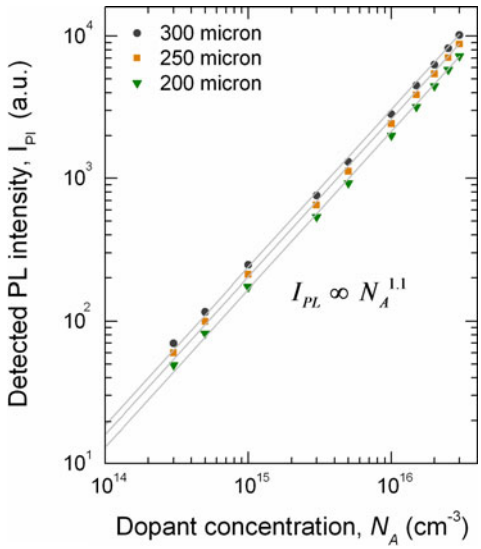

Fig. 1. Modeled results of detected PL intensity as a function of dopant concentration for p-type silicon wafers of three different thicknesses under surface-limited conditions.

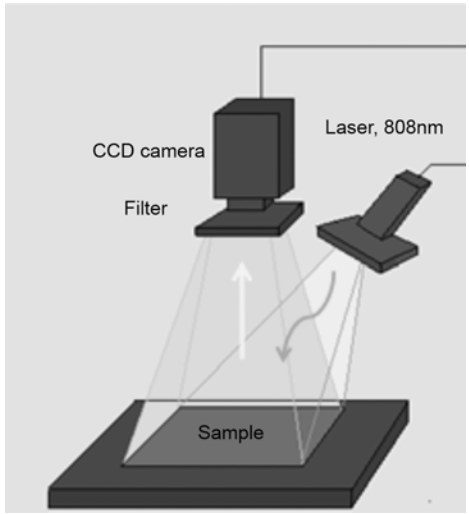

Fig. 2. Schematic diagram of the PL imaging system used in this study.

The band-to-band PL emission is captured with a 1-megapixel silicon charge-coupled device camera with a lateral spatial resolution of 160 μm, allowing the luminescence intensity variation across the sample to be measured. Illumination and detection are from the same side of the sample. During detection, a filter is used to eliminate laser illumination reflected from the sample [1]. A schematic diagram of the imaging tool is shown in Fig. 2. All luminescence imaging was performed under steady-state conditions where the external excitation source is turned ON and held at constant intensity during image acquisition. Images could be taken with variable laser intensity, up to 1-sun equivalent, and with variable integration times from 0.01 to 30 s. The camera that is used in the system is sensitive across part of the spectral range of luminescence corresponding to band-to-band emission from silicon. Unless otherwise stated, all of the images in this study were measured at an incident flux intensity of

2.2×10^{17} photons·cm^{-2}·s^{-1} for an acquisition time of 20 s. Converting PL counts to dopant concentration was performed using the simple power law relationship obtained from the QSS-Model software [9] as described previously, combined with an area-averaged dark conductance measurement performed with an inductive coil.

Since a key requirement of this surface-limited method is the preparation of homogeneous, high recombination active surfaces, the following section demonstrates three sample preparation methods that we have successfully used to obtain the required surface-limited conditions.

A. Aluminum Sputtering

The first approach to achieving surface-limited conditions on silicon samples is through depositing a thin layer of metal, in this case by sputtering aluminum. In this study, 3–4 nm of pure aluminum is sputtered on both sides of the silicon wafers using an RF magnetron sputter coater with the substrate in rotation. The process parameters were a pressure of 3 mTorr, 300 W, and an argon gas flow rate of 35 sccm at room temperature. Sputtering is a useful method to enable a very high surface recombination rate on silicon wafers, including high resistivity wafers. It is also applicable to wafers with any crystal orientation. A drawback of this technique is that some fraction of the incident and emitted light during the PL imaging process is absorbed by the sputtered layer and results in a correspondingly lower intensity measured in the PL images.

B. Deionized Water Etching

The second approach that we have used is by using hot water etching. The roughening effect of hot water has been observed before [11]. We have found in our experiments that this effect can be exploited to generate a homogeneously high surface recombination rate, well suited for our current purpose. This process involves immersing and agitating the silicon wafer in a large beaker of deionized water heated to 65–75 °C for 3–5 min followed by a thorough rinse and blow dry using a nitrogen gun. The process involves the reaction of silicon and its thin native oxide with OH^- ions in the water, leading to the formation of orthosilicic acid, which dissolves and diffuses into the solution [12]. Prolonged etching in deionized water can result in the formation of a residue on the wafer surfaces. This is due to the fact that the mildly acidic solution resulting from the dissolution of orthosilicic acid will inhibit the pH-dependent dissociation process of silicon oxide complexes and result in the polymerization of these complexes, which can be redeposited on the surface [12]. In our experiments, we have observed that a freshly formed residue can be removed by agitating the wafer in a mildly alkaline solution [12] (e.g., 4% aqueous ammonia) heated to about 40 °C. Deionized water etching is found to be effective in achieving a surface recombination velocity in the order of 10^5 cm·s^{-1} for monocrystalline silicon wafers of dopant density above 10^{15} cm^{-3}. In our experiments, this method was found to be effective on monocrystalline wafers of ⟨1 0 0⟩, ⟨1 1 0⟩, and ⟨1 1 1⟩ crystal orientations but not applicable for *mixed* crystal orientation wafers such as multicrystalline wafers, which are roughened to different degrees due to the presence of different crystal orientations.

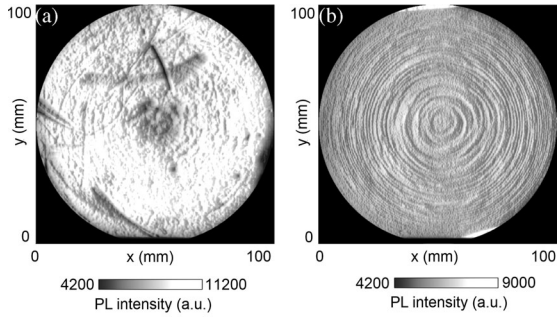

Fig. 3. PL image of a 293-μm-thick, 100-mm-diameter 0.92-Ω.cm n-type FZ silicon wafer measured (a) in as-cut state and (b) after abrasion. Both images are obtained from a single PL measurement using the same laser intensity setting. Note the difference in PL counts scale.

C. Surface Treatment Through Mechanical Abrasions

Another practical approach to achieve surface-limited recombination conditions on silicon wafers is through sand-blasting or sandpaper abrasion. Roughening of the silicon surfaces produces a high concentration of surface defects which facilitates instantaneous recombination of minority carriers. Sand-blasting is preferable to sandpaper abrasion in terms of surface homogeneity. In this study, we have used sandpaper abrasion performed with a sanding block with size slightly larger than the sample to ensure abrasion uniformity, including at the edge of the sample. Microgrit sandpaper of particle size between 15 and 22 μm was used in this experiment, with larger grit size used for the roughening of samples of higher resistivity. In order to reduce the formation of microcracks during the abrasion process, a lubricant such as isopropyl alcohol was applied during the roughening process.

IV. Results and Discussion

A. Comparison of Surface Treatment Methods

Fig. 3(a) and (b) shows the PL images of a 293-μm-thick, 100-mm-diameter phosphorus-doped 0.92-Ω.cm float-zone (FZ) silicon wafer, before and after abrasion, respectively. Distinct concentric rings of dopant density variations can be seen in the PL image measured on the same wafer under surface-limited recombination conditions in Fig. 3(b). In the as-cut state, the PL intensity is more variable, and generally higher, reflecting the poor but detectable surface passivation properties of the native oxide, the effect of which has been removed in the few scratched regions. The passivating effect of this native oxide masks the underlying dopant rings in Fig. 3(a).

Mechanical abrasion is found to be effective for a wide range of silicon samples of various resistivities. Fig. 4 shows the results of measured PL intensity before and after the application of the abrasion for ten phosphorus-doped wafers of various dopant concentrations. The dopant density of the two samples with doping of 6.2×10^{13} and 1.4×10^{14} cm^{-3} was measured using

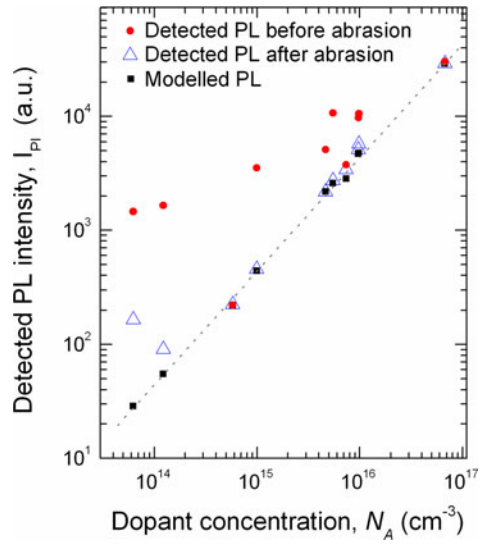

Fig. 4. Results of PL measurements on samples before and after abrasion, and as modeled using the QSSModel [9].

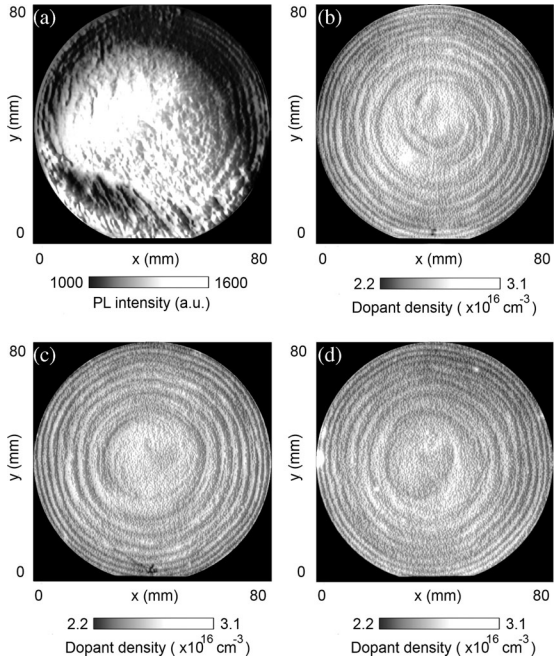

Fig. 5. PL and N_A images of sister wafers of 80-mm diameter, 0.62-Ω.cm boron-doped FZ wafers (a) in as-cut state, (b) after abrasion, (c) after hot water treatment, and (d) after sputtering. The emergence of circular dopant rings of similar structures can be seen in the images of (b), (c), and (d) after surface treatments.

electrochemical capacitance voltage profiling and the remaining samples with dark conductance measurements. The closed red circle symbols represent measured PL intensities from samples before abrasion, the open blue triangle symbols represent the results after abrasion, and the closed black square symbols represent the expected PL intensity for each sample under surface-limited conditions, corresponding to a surface recombination velocity of 1×10^7 cm·s^{-1}, as modeled using the QSSModel software [9]. As the thicknesses of the samples vary in this experiment, the modeled detected PL as a function of dopant density does not exactly follow a single fit, as would be the case for samples with the same thickness. It can be also seen from Fig. 4 that the measured PL intensities of some as-cut samples overlap with the modeled PL, which indicates that the samples are already surface limited in the as-cut state. Large reductions in PL counts can be observed for the rest of the samples after they have attained surface-limited conditions through surface roughening. Due to the fact that lowly doped silicon wafers are more easily passivated by native oxides [13], the measured PL intensity of the least doped samples can be seen to be higher than the modeled intensity after abrasion. This indicates that even after surface abrasion, the surface recombination is not sufficiently high to pin the effective lifetime to the transit time for dopant concentrations below approximately 10^{14} cm^{-3}. Hence, this method is suitable for wafers of dopant density above 5×10^{14} cm^{-3}.

The above surface treatment methods were applied on three sister wafers of 270-μm thickness, 80-mm diameter, and 0.62-Ω.cm resistivity boron-doped FZ silicon. A PL image of a wafer in the as-cut state and calibrated N_A images of each sister wafer treated with different surface treatment methods are shown in Fig. 5(a)–(d), respectively. Very similar concentric dopant density variations are observed in Fig. 5(b)–(d), reflecting the effectiveness of the surface conditions resulting from the three surface preparation treatments. The standard deviations of the PL counts from these samples were 5.1%, 3%, and 4.5%, respectively. The slightly higher deviations found in the abraded and the sputtered samples compared with the sample prepared by the chemical method could be caused by a greater degree of surface nonuniformity resulting from the abrasion process or the sputter coating. From other measurements, it is also observed that samples treated with abrasions or sputtering generally result in a standard deviation of 1–2% higher than those treated through the chemical method. Therefore, such uncertainty should be taken into consideration in the investigation of lateral dopant density variations.

Sheet resistance imaging (SRI) is a dopant imaging technique based on measuring the infrared absorption or emission of free carriers, detected in the 3–5-μm wavelength range [14]. In this study, emission-mode SRI measurements were performed in which the samples were heated to 60 °C, and the infrared light emitted by the free carriers was captured by an infrared camera. SRI has mostly been applied to imaging the sheet resistance of diffused regions [15], but can also be applied to imaging bulk doping. We have applied it here to confirm that our surface-limited images do indeed reflect variations in the base doping and also to allow a comparison of the relative advantages of each method for bulk dopant imaging.

The SRI technique [14], [16] was applied to the abraded and hot-water-treated wafers described above to obtain relative dopant density images, respectively. Fig. 6 shows the resulting images, in which a weak circular pattern can again be observed. These are the same dopant rings seen in the N_A images of Fig. 5. However, the clarity of the SRI images is reduced in comparison with the PL-derived dopant density images, due to a relatively low emission signal. It was also noted that light-trapping effects

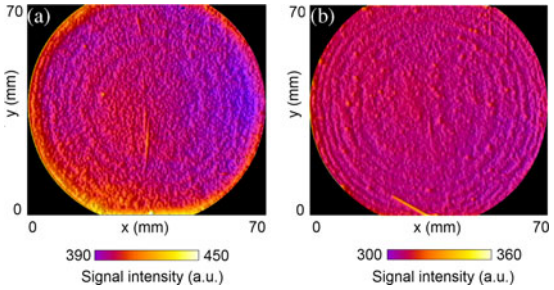

Fig. 6. Dopant density images of (a) abraded and (b) hot water etched boron-doped silicon wafers measured using the SRI technique.

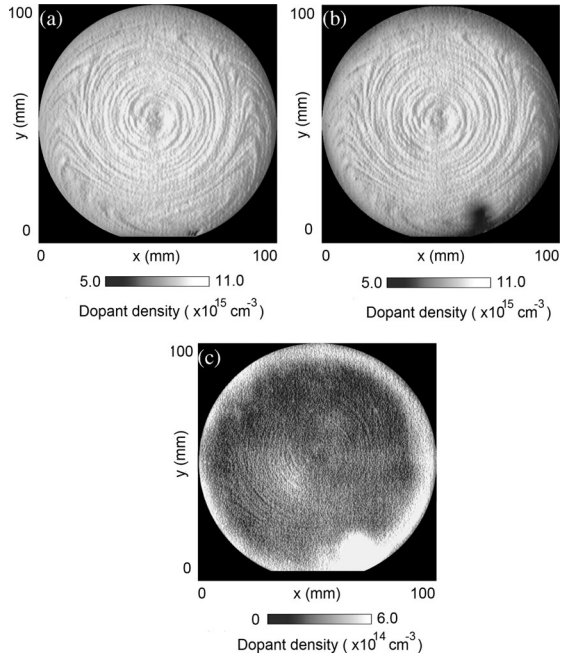

Fig. 7. n and N_D images of a 100-mm-diameter 0.58-Ω.cm phosphorus-doped CZ wafer measured (a) before thermal donor deactivation and (b) after thermal donor deactivation. (c) Thermal donor density image computed from (a) and (b).

resulting from the roughened silicon wafer surfaces caused significant blurring of the SRI images, due to the fact that the detected photons have larger wavelengths than those used in the PL method (3–5 μm compared with around 1 μm), and are, therefore, very weakly absorbed in Si. Slightly clearer structures are seen from the hot-water-treated sample, which had a smoother surface, and, therefore, caused a lesser degree of light trapping within the wafer. Despite the difference in image quality, N_A images from both the surface-limited and SRI techniques revealed reasonably good qualitative agreement, confirming that the observed rings are indeed due to dopant density variations.

B. Thermal Donor Imaging

Oxygen is introduced unintentionally in silicon ingots during crystal growth process. At temperatures around 450 °C, oxygen atoms become mobile. Silicon vacancies containing two or more oxygen atoms have been considered as possible candidates for thermal donors [17], [18]. Unlike standard dopants, thermal donors can introduce multiple energy levels in the bandgap, leading to a double donor behavior [19].

Thermal donors can influence the net dopant concentration in material that is not heavily doped, by adding to or compensating the other dopants present. For an n-type sample, the thermal donor density *[TD]* can be computed based on the following expression assuming all thermal donors are double donors [19]:

$$n_0 = N_D^+ + 2 \times [TD] \tag{4}$$

where n_0 is the majority carrier (electron) density before thermal donor deactivation, and N_D^+ is the phosphorus concentration, which is then equal to the electron density after thermal donor deactivation. Detailed information on the properties of thermal donors in silicon can be found in [17] and [18]. The undesirable effects introduced by the thermal donors can be effectively deactivated through high-temperature annealing of 650 °C for 30 min [19]. Postannealing density measurement, hence, reflects onlyN_D^+. By obtaining n_o before and after the deactivation process, $[TD]$can be subsequently determined. Spatial information of $[TD]$ in particular provides knowledge that leads to a better understanding of the oxygen sources in silicon ingots.

In this section, the surface-limited net dopant imaging technique is applied to the measurement of thermal donor concentration in Czochralski (CZ)-grown silicon wafers. The sample used in this section was a 290-μm-thick, 100-mm-diameter, 0.58-Ω.cm phosphorus-doped silicon wafer. Surface-limited conditions were achieved by using hot water etching. By determining n_0 and $N_D^+$with net doping images measured in the as-cut state of the sample and after thermal donor annealing, both under surface-limited conditions and at the same temperature, an image of the thermal donor concentration can, in principle, be computed. Thermal donor annealing was carried out at 650 °C under N_2 flow for 30 min. Fig. 7(a) and (b) shows the n_0 and N_D^+ images. Both images showed similar doping structures. Fig. 7(c) shows the thermal donor density image derived from the difference of the previous two images. The dark spot at the lower right region in Fig. 7(b) is due to contamination resulting from the scribed wafer label, which diffused into the surrounding area after high-temperature treatment. The bright spot in the same location observed in Fig. 7(c) is the artifact resulting from that local contamination. Cross-sectional line scans for all three images are shown in Fig. 8. From Figs. 7 and 8, it can be observed that the thermal donor concentration is higher at the periphery and relatively uniform in the inner region of the wafer. The higher concentration at the edge was measured to be 4–6% of the base dopant concentration and below 1% of the base dopant concentration for the rest of the wafer. This thermal donor distribution reveals an oxygen-rich layer at the periphery of the ingot. Similar oxygen-rich profiles at the edges of CZ wafers have been observed by Witting through applying line-scanned Fourier transform infrared spectroscopy (FTIR) measurements [20]. Due to the relationship between the thermal donor concentration and the interstitial oxygen concentration, this approach can, in principle, be used to generate $[O_i]$imaging [19].

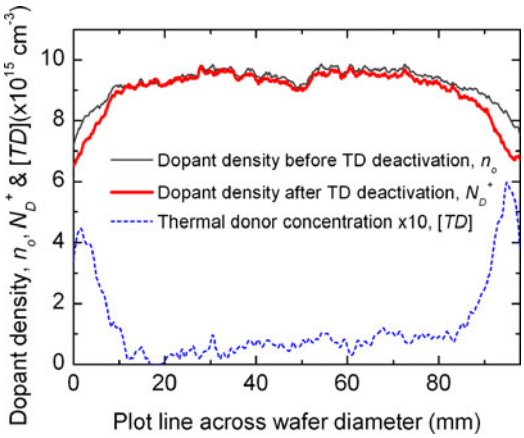

Fig. 8. Thermal donor concentration derived from dopant density line scans before and after thermal deactivation, showing an increase near in the edge.

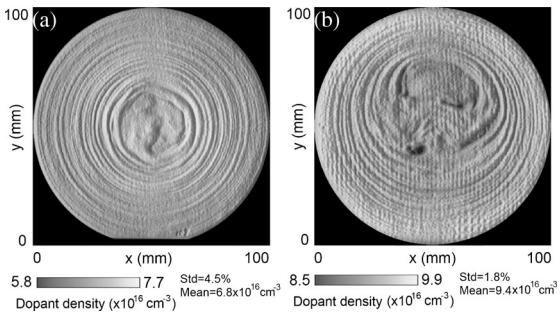

Fig. 9. Dopant images of surface-limited samples. (a) 0.11-Ω.cm phosphorus-doped FZ silicon wafer. (b) 0.21-Ω.cm boron-doped FZ silicon wafer.

C. Radial Dopant Density Variation in Czochralski and Float-Zone Silicon Wafers

The surface-limited net doping imaging technique can be used to evaluate radial dopant density variations in silicon wafers, which can be useful for ingot growth monitoring and optimization. Sixteen randomly chosen CZ- and FZ-grown samples of different doping concentrations were used in this experiment. All CZ-grown wafers were also subjected to thermal donor deactivation through 660 °C annealing for 30 min. DI water etching was used to achieve surface-limited recombination conditions on the samples. Our results showed higher standard deviations in CZ-grown silicon wafer (boron-doped: 3.3–5.6%; phosphorus-doped 5.0–9.4%) than FZ-grown wafers (boron-doped: 1.7–4.0%; phosphorus-doped: 3.1–5.0%). It can also be observed in both cases that higher deviation is found in phosphorus-doped than boron-doped silicon wafers. This suggests an influence of the segregation coefficient of the dopant impurity and the effect of the presence of a nonplanar freezing interface during ingot solidification [21]. Fig. 9(a) and (b) shows the dopant density images of 100-mm-diameter phosphorus- and boron-doped FZ silicon wafers, respectively. Concentric structures of dopant density of various widths can be seen. Some uneven structures apparent in the centre region could be due to fluctuations or turbulence effects in the melt neck during the crystallization process. Similarly, from the phosphorus-doped CZ silicon sample in Fig. 7(a), some noncircular-shaped variations of dopant concentration can also be observed in the outer area of the ingot, suggesting local thermal fluctuations in the melt during crystal solidification.

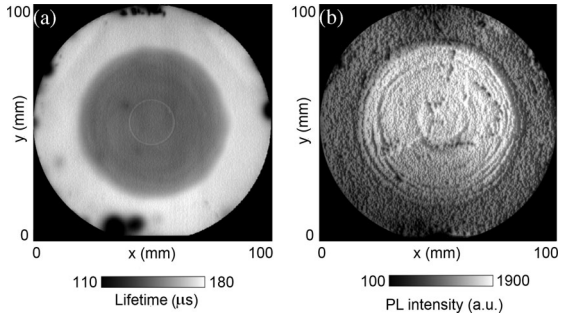

Fig. 10. (a) Lifetime of a passivated 100-mm-diameter phosphorus-doped 3000-Ω.cm FZ wafer calibrated with QSSPC coil based on uniform base dopant density. (b) PL image of the same wafer measured under surface-limited conditions after aluminum sputtering, reflecting a count rate which is two times higher in the central region than in the peripheral region.

D. Donor-Related Defects in High-Resistivity Phosphorus-Doped Float-Zone Silicon Wafers

We have regularly observed circular regions with low PL counts in the center of high-resistivity n-type FZ silicon wafers that have received high-temperature processing. A similar effect has also been reported in p-type CZ wafers [22]. In principle, such low PL regions can be caused by either increased recombination or reduced doping, for example, by changing thermal donor concentrations. Here, we show that a comparison of dopant images obtained by the surface-limited method, and lifetime images obtained on passivated samples, allows the relative impact of changes in recombination and doping to be compared. Fig. 10(a) shows the calibrated excess carrier lifetime image of a passivated 494-μm-thick, 100-mm-diameter phosphorus-doped FZ wafer of 3000 Ω.cm measured with a laser flux intensity of 1.17×10^{17} photons.cm^{-2}·s^{-1} for 2 s. The sample was passivated with thermally grown silicon oxide grown at 950 °C for 30 min. The high-temperature process also caused deactivation of thermal donors. An apparent strong reduction of lifetime in the central region of the wafer is evident. Note that the single thin bright ring in the center of Fig. 10(a) is actually an artefact caused by reflection from an inductive coil below the sample.

The sample then underwent an HF dip to remove the thermal oxide layer on both sides for thorough cleaning and aluminum sputtering to create high surface recombination velocities. Fig. 10(b) shows that the resultant PL image of the sample under surface-limited conditions (confirmed by quasi-steady-state photoconductance (QSSPC) lifetime measurement). A higher majority carrier density was observed in the central region of the wafer, which corresponds to the region where the stark reduction of lifetime was found in the passivated case [see Fig. 10(a)]. Note that the circular structures in the surface-limited case are observed to be related to doping rather than carrier lifetime, as they were not evident in the image of Fig. 10(a), where the detected PL intensity was orders of magnitude higher. The above results point to the fact that the central region contains

both a recombination active defect and a greater concentration of donors, which may or may not be caused by the same physical defect. Schulze and Kolbesen have also reported the presence of such defects in crystalline silicon and suggested that they are related to vacancy clusters formed during crystal growth, which become active after high-temperature treatment [23].

V. Conclusion

Three surface preparation methods to enable direct determination of PL-based dopant density images have been demonstrated. The first approach, i.e., aluminum sputtering, is capable of generating reliable, high surface recombination velocities, even on high-resistivity samples, and also on any crystal orientation. The second approach, i.e., hot deionized water etching, is a simple and effective method which yields higher surface uniformity, but it is only applicable to monocrystalline silicon wafers. The third method that is based on mechanical abrasion is applicable to both monocrystalline and multicrystalline silicon wafers, due to its independence on sample crystal orientation. Dopant density images obtained from samples treated with these methods were verified with results obtained using SRI. Three applications of the technique were also demonstrated in this paper. A first application involves thermal donor imaging, through which useful information can be obtained to understand oxygen distributions and dopant incorporation in silicon ingots. The second application investigated lateral dopant density variation on FZ- and CZ-grown monocrystalline silicon wafers. Finally, dopant density imaging is also shown to be useful for comparing with PL-based lifetime images, in assessing the relative importance of variations in recombination or the net doping.

Acknowledgment

The authors would like to thank M. Brauers of the Australian National University for assisting with wafer preparations.

References

[1] T. Trupke, R. A. Bardos, M. C. Schubert, and W. Warta, "Photoluminescence imaging of silicon wafers," *Appl. Phys. Lett.*, vol. 89, pp. 044107-1–044107-3, 2006.

[2] S. Y. Lim, S. P. Phang, T. Trupke, A. Cuevas, and D. Macdonald, "Dopant concentration imaging in crystalline silicon wafers by band-to-band photoluminescence," *J. Appl. Phys.*, vol. 110, pp. 113712-1–113712-7, 2011.

[3] F. D. Heinz, W. Warta, and M. C. Schubert, "Doping density in silicon and solar cells analyzed with micrometer resolution," *IEEE J. Photovoltaics*, vol. PP, pp. 1–7.

[4] T. Trupke and R. A. Bardos, "Photoluminescence: A surprisingly sensitive lifetime technique," in *Proc. 31st IEEE Photovoltaic Spec. Conf.*, Orlando, FL, Jan. 2005, pp. 903–906.

[5] M. Boulou and D. Bois, "Cathodoluminescence measurements of the minority carrier lifetime in semiconductors," *J. Appl. Phys.*, vol. 48, pp. 4713–4721, 1977.

[6] A. Cuevas and R. A. Sinton, "Prediction of the open-circuit voltage of solar cells from the steady-state photoconductance," *Progr. Photovoltaics: Res. Appl.*, vol. 5, pp. 79–90, 1997.

[7] A. B. Sproul, M. A. Green, and A. W. Stephens, "Accurate determination of minority carrier and lattice scattering mobility in silicon from photoconductance decay," *J. Appl. Phys.*, vol. 72, pp. 4161–4171, 1992.

[8] P. P. Altermatt, F. Geelhaar, T. Trupke, X. Dai, and A. Neisser, "Injection dependence of spontaneous radiative recombination in crystalline silicon: Experimental verification and theoretical analysis," *Appl. Phys. Lett.*, vol. 88, pp. 261901-1–261901-3, 2006.

[9] A. Cuevas, "Modelling silicon characterisation," *Energy Procedia*, vol. 8, pp. 94–99, 2011.

[10] B. Mitchell, T. Trupke, J. W. Weber, and J. Hyhus, "Bulk minority carrier lifetimes and doping of silicon bricks from photoluminescence intensity ratios," *J. Appl. Phys.*, vol. 109, pp. 083111-1–083111-12, 2011.

[11] J. H. Eisenberg, S. F. Shive, F. Stevie, G. S. Higashi, T. Boone, K. Hanson, J. B. Sapjeta, G. N. Dibello, and K. L. Fulford, "Effect of hot water exposure on bare silicon surfaces in MOS processing," *MRS Proc.*, vol. 315, pp. 485–490, 1993.

[12] H. Seidel, L. Csepregi, A. Heuberger, and H. Baumgartel, "Anisotropic etching of crystalline silicon in alkaline solutions," *J. Electrochem. Soc.*, vol. 137, pp. 3626–3632, 1990.

[13] H. Mackel and A. Cuevas, "Determination of the surface recombination velocity of unpassivated silicon from spectral photoconductance," in *Proc. 3rd World Conf. Photovoltaic Energy Convers.*, Osaka, Japan, 2003, pp. 71–74.

[14] M. C. Schubert, J. Isenberg, and W. Warta, "Spatially resolved lifetime imaging of silicon wafers by measurement of infrared emission," *J. Appl. Phys.*, vol. 94, pp. 4139-1–4139-5, 2003.

[15] J. Isenberg, S. Riepe, S. W. Glunz, and W. Warta, "Carrier density imaging (CDI): A spatially resolved lifetime measurement suitable for in-line process-control," in *Proc. 29th IEEE Photovoltaic Spec. Conf.*, New Orleans, LA, 2002, pp. 266–269.

[16] J. Isenberg, D. Biro, and W. Warta, "Fast, contactless and spatially resolved measurement of sheet resistance by an infrared method," *Progr. Photovoltaics: Res. Appl.*, vol. 12, pp. 539–552, 2004.

[17] D. J. Chadi, "Core structure of thermal donors in silicon," *Phys. Rev. Lett.*, vol. 77, pp. 861–864, 1996.

[18] U. Gosele and T. Y. Tan, "Oxygen diffusion and thermal donor formation in silicon," *Appl. Phys. A*, vol. 28, pp. 79–92, 1982.

[19] J. Veirman, S. Dubois, N. Enjalbert, and M. Lemiti, "A fast and easily implemented method for interstitial oxygen concentration mapping through the activation of thermal donors in silicon," *Energy Procedia*, vol. 8, pp. 41–46, 2011.

[20] I. T. Witting, "Defect and impurity distributions in traditionally cast multicrystalline and cast monocrystalline silicon for solar subtrates," Master thesis, Raleigh Univ., Raleigh, 2008.

[21] W. Zulehner, "Status and future of silicon crystal growth," *Mater. Sci. Eng.*, vol. B04, pp. 1–10, 1989.

[22] J. Haunschild, I. E. Reis, J. Geilker, and S. Rein, "Detecting efficiency-limiting defects in Czochralski-grown silicon wafers in solar cell production using photoluminescence imaging," *Phys. Status Solidi (RRL)*, vol. 5, pp. 199–201, 2011.

[23] H. J. Schulze and B. O. Kolbesen, "Influence of silicon crystal defects and contamination on the electrical behaviour of power devices," *Solid -State Electron.*, vol. 42, pp. 2187–2197, 1998.

Authors' photographs and biographies not available at the time of publication.